Influence of mix design on the carbonation, mechanical properties and microstructure of reactive MgO cement-based concrete

S. Ruan[a], C. Unluer[a,*]

[a] School of Civil and Environmental Engineering, Nanyang Technological University, 50 Nanyang Avenue, Singapore 639798

* Corresponding author. Tel.: +65 91964970, E-mail: ucise@ntu.edu.sg

Abstract

This study assesses the influence of mix design on the hydration and carbonation of reactive MgO cement (RMC)-based concrete formulations by varying the water and cement contents. Samples were subjected to accelerated carbonation under 10% CO_2 for up to 28 days and compared with corresponding PC-based samples. Their performance was analyzed by compressive strength, porosity, density, water sorptivity and thermal conductivity measurements. XRD, TGA/DSC and FESEM/SEM analyses were employed to investigate the formation of hydration and carbonation products and microstructural development. RMC samples achieved 28-day strengths of 62 MPa, which was comparable with PC samples. Strength gain of RMC samples was accompanied with a substantial decrease in porosity, determined by the amount and morphology of carbonates. The initial water content was more influential on final performance and thermal conductivity than cement content. Lower water contents led to higher strengths due to lower porosities and faster CO_2 diffusion within dry mediums.

Keywords: Reactive MgO cement; hydration; carbonation; porosity; strength; microstructure

1. Introduction

The increase in the concentration of greenhouse gases in the atmosphere due to human activity has given rise to climate change, which is regarded as a major environmental concern [1]. Portland cement (PC) production is responsible for 5-7% of the total global anthropogenic carbon dioxide (CO_2) emissions [2]. This has led to the development of practices and products that are associated with lower CO_2 emissions than traditional approaches. Some of these include the reduction of energy used during PC production, replacement of PC with waste materials or industrial by-products such as supplementary cementitious materials (SCMs) and the development of alternative binders [3-5]. However, these practices are not fully sufficient in mitigating the impacts of PC production and concrete use within the construction industry due to prominent reasons such as the high costs involved in the development of new technologies and insufficient supply of certain by-products in different parts of the world. This has paved the way for the development of alternative construction materials that could potentially offer reduced CO_2 emissions.

Reactive magnesia (MgO) cement (RMC), which was developed more than a decade ago [6, 7], has gained attention due to the lower temperatures used during its production (750 vs. 1450 °C for PC) and ability to gain strength via carbonation [7]. The use of RMC has been proposed in a variety of cement-based applications in which it can be used as the sole binder or along with PC and/or pozzolans. Unlike PC mixes, which mainly rely on the hydration process for strength gain, RMC-based formulations gain strength and achieve stiffness through carbonation [8-11]. The chemical reactions that take place within these mixes, as listed below in Equations 1-5, can be summarized in two main steps: (i) hydration of RMC to form brucite ($Mg(OH)_2$) and (ii) reaction of brucite with CO_2 to form a range of hydrated magnesium carbonates (HMCs). Some of main HMCs that have been observed within RMC-based mixes are nesquehonite ($MgCO_3 \cdot 3H_2O$), hydromagnesite ($4MgCO_3 \cdot Mg(OH)_2 \cdot 4H_2O$), dypingite ($4MgCO_3 \cdot Mg(OH)_2 \cdot 5H_2O$) and artinite ($MgCO_3 \cdot Mg(OH)_2 \cdot 3H_2O$) [9, 12, 13].

$MgO + H_2O \rightarrow Mg(OH)_2$ (brucite) (1)

$Mg(OH)_2 + CO_2 + 2H_2O \rightarrow MgCO_3 \cdot 3H_2O$ (nesquehonite) (2)

$5Mg(OH)_2 + 4CO_2 \rightarrow 4MgCO_3 \cdot Mg(OH)_2 \cdot 4H_2O$ (hydromagnesite) (3)

$5Mg(OH)_2 + 4CO_2 + H_2O \rightarrow 4MgCO_3 \cdot Mg(OH)_2 \cdot 5H_2O$ (dypingite) (4)

$2Mg(OH)_2 + CO_2 + 2H_2O \rightarrow MgCO_3 \cdot Mg(OH)_2 \cdot 3H_2O$ (artinite) (5)

As the strength gain mechanism of RMC-based binders are directly dependent on carbonation, it is critical to understand the steps involved during this process. The carbonation of concrete mixes involves the: (i) Diffusion of CO_2 into the unsaturated pore network, (ii) penetration and dissolution of CO_2 within the pore system, (iii) formation of carbonic acid (H_2CO_3) in the pore solution, (iv) ionization of carbonic acid and emergence of H^+ and CO_3^{2-}, (v) leaching of Mg^{2+} from the dissolution of $Mg(OH)_2$ crystals and (vi) formation of HMCs via the reaction between Mg^{2+} and CO_3^{2-}.

The rate and degree of the carbonation reaction, along with the morphology of the carbonate phases determine the final performance of RMC-based mixes. The main reason behind strength development is attributed to two main factors. The first one is the reduction of the initial porosity as carbonation is an expansive process that reduces the overall pore volume (i.e. the formation of HMCs causes a significant expansion and increases the solid volume by a factor of 1.8-3.1). This is supported by the microstructure evolution as the morphology and binding strength of the carbonate crystals contribute to the network structure.

Several studies have reported the importance of the morphology of carbonates, rather than their amount, as the main factor in determining final performance [14, 15]. HMCs have microstructures with varying morphologies that add microstructural strength to cement formulations due to their strong, fibrous, acicular or elongated nature via the

interlocking effects occurring between the crystals. Fibrous and needle-like crystal growths established by HMCs are more beneficial than rounded or tabular crystals because of the 3D structures formed. The compact and interlocked network-like structures established by interconnected and well-developed crystals control the overall performance [15]. This is further supported by the bulk “micro-aggregate” formed through localized carbonation, which also contributes to the creation of a dense matrix [14].

Unlike the less reactive forms of MgO (i.e. hard- or dead-burned) that are produced at much higher temperatures, RMC hydrates at a similar rate to PC, thus eliminating the expansion problems [8]. In addition to the properties of RMC determined by the production conditions (e.g. calcination temperature and residence time), some of the major factors that control the rate and degree of carbonation of RMC are mix design (e.g. water, cement and aggregate contents) and curing conditions (e.g. relative humidity, temperature and CO_2 concentration and pressure) [12, 16-19]. Comprehending the influence of these factors on the strength development of RMC mixes can lead to the development of formulations with maximum carbonation and associated mechanical performance.

Similar to PC mixes, the initial water content plays an important role in the strength development of RMC mixes as water provides a medium for the hydration and carbonation reactions [12, 20]. Increasing the water content of concrete mixes can increase the capillary porosity and improve the interconnectivity of voids, thereby enhancing the carbonation process [21, 22]. Meanwhile, the presence of excess water can inhibit the diffusion of CO_2 within the pore system, thereby slowing down carbonation. The optimization of the water content is critical as low water/cement (w/c) ratios can lead to poor compaction and crumbling, whereas high w/c ratios can reduce the CO_2 diffusivity and therefore hinder the formation of HMCs and associated strength development within RMC mixes [12].

Another factor that can influence the strength development of RMC-based concrete mixes is the cement content (i.e. aggregate/cement ratio) [23, 24]. As the carbonation of RMC mixes involves a series of reactions within the MgO-CO_2-H_2O system, an increase in the cement content can potentially lead to an increase in the amount of final hydrate and carbonate phases. However, this can also lead to the decrease of initial porosity as the fine cement particles fill in the available pores between the coarse aggregates. While this would lead to increased strength in PC mixes that rely on the hydration process for strength gain, the provision of a sufficiently high porosity within the initial mix design via the use of a high aggregate content is essential for the continuation of the carbonation reaction within RMC mixes. Therefore, the optimization of the aggregate/cement ratio is important for the enhancement of gas diffusivity and permeability [25]. Along with the aggregate/cement ratio, the amount and the saturation level of aggregates can determine the effective water content within a mix. Increasing the amount of aggregates can alleviate shrinkage and bleeding and therefore improve the bond between the aggregates and cement paste [5], whereas high aggregate contents eventually lead to lowered strengths due to the corresponding reductions in the cement content [26].

This paper aims to assess the influence of mix design via a variation of the water and cement contents on the hydration and carbonation potential of RMC-based concrete formulations. The extent of these reactions and the morphology of the resulting phases, which determine the mechanical performance and microstructural development of the prepared samples, were evaluated. RMC-based concrete samples were subjected to accelerated carbonation at a 10% CO_2 concentration for up to 28 days. Corresponding PC-based samples, which were hydrated for the same duration to enable maximum strength gain, were prepared for comparison purposes. The performance of the prepared samples was analyzed at different durations by compressive strength testing as well as porosity, density, water sorptivity and thermal conductivity measurements. X-ray diffraction (XRD), thermogravimetric analysis and differential scanning calorimetry (TGA/DSC), field emission scanning electron microscopy (FESEM) and scanning electron microscopy (SEM) analyses were employed to analyze the formation of

hydration and carbonation products and investigate the microstructure development at the end of the curing process.

2. Materials and Methodology

2.1. Materials, mix composition and sample preparation

The main cement binder used in this study was RMC (commercial name “calcined magnesite 92/200”) obtained from Richard Baker Harrison Ltd. (UK). Ordinary PC obtained from Lafarge cement Pte. Ltd. (Singapore) was used in the preparation of the PC-based control samples. The chemical and physical properties of RMC and PC as provided by the suppliers are listed Table 1. Coarse aggregates with a particle size of 4.7-9.5 mm supplied by Buildmate Pte. Ltd. (Singapore) was used to form the aggregate profile in the prepared concrete samples.

The standard consistency (SC) of RMC and PC were measured according to BS EN 196-3 as ~0.60 and 0.33, respectively [27]. This led to the preparation of RMC and PC control samples containing 40% cement and 60% aggregates at w/c ratios of 0.60 and 0.33, respectively. Concrete samples were prepared by mixing the dry components first, followed with the addition of water to the dry mix. To study the effect of water content, RMC samples with two different w/c ratios corresponding to SC±8.3% were prepared. The effect of cement content was studied by changing it by ±12.5%. All the mix compositions used in this study are listed in Table 2.

The prepared mixes were then cast into 50×50×50 mm cubic molds, consolidated by a vibrating table and trowel finished. All samples were demolded after 24 hours and placed into respective curing environments for up to 28 days. The demolded RMC samples were subjected to accelerated carbonation (28±2 °C, 80±5% RH, 10% CO_2).

Corresponding PC-based control samples were cured under water or in air (28±2 °C, 80±5% RH, ambient CO_2) to achieve maximum strength gain for comparison purposes.

2.2. Methodology

2.2.1. Density and porosity

The mass of each sample was recorded before and after curing to measure the change in mass due to hydration and/or carbonation. Densities of samples at different curing periods were calculated by recording their masses, which was performed in triplicates. Similarly, the porosities of the samples before and after curing were calculated via Equation 6, where m_{sat} is the sample mass saturated in water, m_{dry} is the sample mass dried at 70 °C and v is the sample volume.

$$p = \frac{m_{sat} - m_{dry}}{v} * 100 \quad (6)$$

2.2.2. Water sorptivity

The prepared samples were tested for their water sorptivity before and after curing according to ASTM C1585-04 [28]. To enable this, the cubic concrete samples were dried in oven set at 70 °C for 3 days, after which they were cooled under room temperature and coated with epoxy on the sides. The size of the concrete surface in contact with water, i.e. the inflow surface, was 50 x 50 mm. The mass of each sample was recorded at various times using an electronic balance. Water absorption (I) was calculated by dividing the change in mass (Δm) with the concrete inflow surface area (a) and density of water (ρ), as shown in Equation 7. The initial rate of water absorption (k,

mm/seconds$^{1/2}$) was stipulated as the slope of the line that was the best fit to water absorption (I) plotted against the square root of time (t, seconds), as shown in Equation 8.

$$I = \frac{\Delta m}{a * \rho} \quad (7)$$

$$I = k * t^{0.5} \quad (8)$$

2.2.3. Compressive strength

The compressive strength of the prepared concrete samples were measured by uni-axial loading in triplicates at 7, 14 and 28 days in accordance with the specifications of ASTM C109/C109M – 13 [29]. The equipment used for this purpose was a Toni Technik Baustoffprüfsysteme machine, operated at a loading rate of 55 kN/min.

2.2.4. XRD, TGA/DSC, FESEM and SEM analyses

Samples extracted from the cubes crushed during strength testing were stored in acetone to stop hydration, followed by vacuum drying in preparation for x-ray diffraction (XRD), thermogravimetric analysis and differential scanning calorimetry (TGA/DSC), field emission scanning electron microscopy (FESEM) and scanning electron microscopy (SEM) analyses. The dried samples were ground down to pass through a 125 µm sieve before they were analysed under XRD and TGA/DSC. XRD was recorded on a Philips PW 1800 spectrometer using Cu Kα radiation (40 kV, 40 mA) with a scanning rate of 2° 2θ/step from 5 to 80° 2θ. Phase quantification was performed via the Rietveld refinement software TOPAS 5.0 with fundamental parameter approach [30].

TGA/DSC was conducted on a Perkin Elmer TGA 4000 equipment from 40 to 900 °C with a heating rate of 10 °C/min under nitrogen flow. The dried samples were mounted onto aluminum stubs using double-sided adhesive carbon disks and coated with gold before SEM analysis. The microstructural analysis of representative specimens was investigated by imaging fracture surfaces by FESEM and SEM. The analysis was carried out with a Zeiss Evo 50 microscope with the goal of evaluating the morphologies of the hydration and carbonation products and facilitating elemental composition analysis within the prepared samples.

2.2.5. Thermal conductivity

Thermal conductivity measurements were conducted using a transient plane source Thermal Constants Analyser (model TPS 500) to assess the influence of the studied parameters on the capacity of the prepared samples to conduct heat [31]. To enable this, a 3.189 mm Kapton disk type sensor was sandwiched between two 50x50x50 mm samples. The measurement time and the heating power were set to 5 seconds and 70 mW, respectively. All tests were conducted at a room temperature of 23 °C.

3. Results

3.1. Density and porosity

Fig. 1 shows the change in the densities of all samples cured for up to 28 days, which can provide a rough estimation of the extent of carbonation within the samples. Most of the samples demonstrated a constant increase in their density with curing age, which was associated with the progress of the hydration and carbonation reactions. These

reactions enabled the reduction of the initial porosities and an associated increase in sample densities via the expansive nature of the hydrate and carbonate phases, whose formation led to the filling up of the initially available pore space. RMC samples revealed a higher increase in density over the PC samples (i.e. 4-7% vs. 0-2% at 28 days). This was associated with the formation of carbonate phases over the entire curing period. The highest increase in density was observed during the first 7 days of curing, which happened at a lower rate in subsequent curing durations, showing that the reactions slowed down after 7 days. The highest percentage increase in density reaching up to 7% over 28 days was revealed by the control sample M40-0.6, along with samples M40-0.55 and M45-0.6.

A reduction in the water content from a w/c ratio of 0.6 to 0.55 led to the highest increase in density at early ages (≤ 7 days). This was attributed to the faster diffusion of CO_2 through less saturated mediums. The opposite effect was observed when the w/c was increased to 0.65, leading to a slower diffusion of CO_2, which was reflected as a lower increase in density over the entire curing period. The higher contents of water in concrete samples can inhibit the diffusion of CO_2, thereby reducing the rate of the carbonation reaction and associated increase in density [9, 12]. Another factor to consider is the evaporation of water within the samples, which can increase with increased water contents (i.e. assuming all other parameters such as temperature, humidity and wind velocity are kept constant) [32, 33]. This may have led to an increased evaporation degree in sample M40-0.65, which can cause a reduction in sample mass and density.

Samples with different cement contents ranging from 35 to 45% revealed similar densities during the entire course of carbonation. A slight increase in density was observed with an increase in the cement content of sample M45-0.6 and vice versa. This may be due to the carbonation potential of the cement powder, whose content within the overall concrete mix design not only influences the initial density due to its fine nature, but also the diffusion rate of CO_2 and the overall degree of carbonation. Although aggregates occupy a majority of the sample volume, their role in the

carbonation process is secondary as their imperfect packing arrangement merely provides the necessary porosity for the diffusion of CO_2 within the sample pore system. The formation of hydrate and carbonate phases is mainly dependent on the properties of the cement paste and pore structure, where the reaction between brucite and CO_2 takes place as shown in Equations 2-5. An optimum cement content that does not block the continuous ingress of CO_2 by filling up the available pore network can facilitate the carbonation reaction via increased amount of reactants. This can explain the higher increase in the density of sample M45-0.6 as opposed to samples with lower cement contents.

The porosities of all samples cured for up to 28 days are shown in Fig. 2. In line with the increase in densities, a reduction in the porosities of all RMC samples was observed as carbonation progressed. Initial porosities of RMC samples before carbonation ranged between 23-31%, whereas PC samples revealed a porosity of 10% before carbonation. Similar to the density results, the porosities of PC samples did not indicate a major change over the 28 days of curing, while RMC samples achieved porosities of as low as 7-11% due the formation of carbonate phases. Unlike RMC samples, the lack of a major change in the porosities of PC samples was due to the different curing mechanisms samples containing these two binders were exposed to (i.e. hydration vs. carbonation). As evident from the overall density and porosity data, PC samples revealed almost constant porosities along the entire curing process as their strength gain mechanism was due to the hydration process, resulting in a small reduction in porosity.

Alternatively, RMC samples demonstrated an up to 21% decrease in their porosities at 28 days. It was mainly the expansive formation of HMCs that resulted in this significant reduction in the initial porosities of RMC samples [9, 12], which revealed very similar or even lower porosity results than PC samples at the end of the 28-day curing period. In line with the density results, a majority of the porosity reduction took place during the first 7 days of curing as the carbonation reaction slowed down afterwards. This was attributed to the slower diffusion of CO_2 after the formation of a dense carbonate network within the initially available pore space. The initially formed HMCs can form a

dense layer around the MgO and brucite crystals, hindering further access of CO_2 to the uncarbonated hydrate phases [34]. This results in the reduction of the rate of porosity change, which stabilizes once the carbonation reaction ceases.

RMC samples with reduced water contents (M40-0.55) revealed lower initial porosities as expected, since the water content controlled the capillary porosity of concrete samples. An increase in the w/c ratio from 0.55 to 0.6 led to an increase in the initial porosity from 23 to 31%. The initial water content of samples also influenced the change in their porosities, which was an indication of the extent of carbonation. Sample M40-0.6 revealed a higher change in porosity than M40-0.55 and M40-0.65, potentially because of a higher degree of brucite and HMC formation due to CO_2 absorption. When compared to the water content, the effect of cement content on porosity was less pronounced. Sample M35-0.6 indicated a lower porosity than the corresponding samples with higher cement contents, M40-0.6 and M45-0.6, which possessed similar porosities at all curing durations. The slightly lower porosity of M35-0.6 could be attributed to the higher aggregate content of this particular sample, which may have absorbed some of the unbound water to achieve saturation. This may have resulted in the reduction of the effective water content and thereby the initial porosity of this particular sample [23, 24].

3.2. Water sorptivity

Measurements of water sorptivity were performed to assess the capillary suction of unsaturated concrete samples with different compositions when placed in contact with water [5]. The results obtained by this measurement could be an indication of the carbonation ability of each sample as water ingress could reflect the pore structure and provide an indirect approach of the measurement of interconnected capillary pores [35]. The main output of this test was the initial rate of water absorption of samples before

and after 7 days of curing (i.e. the slope of the second rate of water absorption was almost zero), as reported in Fig. 3.

All samples experienced a significant reduction in their water sorptivity values after hydration and carbonation due to the densification of their microstructures. This was enabled via the formation of hydrate and carbonate phases during the measured time frame [14]. PC samples indicated a much lower water sorptivity than corresponding RMC samples before the curing process. This difference between the sorptivity values of RMC and PC samples greatly diminished after curing. The progress of hydration within the PC samples led to a reduction in the capillary pore space over time, thereby reducing their water sorptivity [36].

Out of all the RMC samples, sample M40-0.55 demonstrated the lowest water sorptivity values before carbonation (i.e. up to 60% lower than corresponding samples with higher water contents), owing to its relatively lower initial capillary porosity. These results were in agreement with the porosity values presented in Fig. 2, outlining PC samples for their much lower porosities than RMC samples and M40-0.55 for its lower porosity than all other RMC samples. The introduction of carbonation to sample M40-0.55 reduced its water sorptivity to a value slightly higher than the corresponding measurement of M40-0.6. This could be an indication of the slightly lower hydration/carbonation of sample M40-0.55 when compared to M40-0.6.

When samples with different cement contents were compared, sample M35-0.6 revealed a lower water sorptivity than the corresponding samples M40-0.6 and M45-0.6, which was in line with the porosity results. This could be attributed to the smaller paste and thereby the lower capillary pore content within this sample when compared to samples with higher cement contents. A similar finding was reported by previous studies [37], who highlighted the link between capillary absorption and volume of cement paste, as well as the water content. A higher capillary absorption is expected in samples with higher water contents and paste volumes, when all the other parameters are kept constant. Overall, the results were in agreement with previous findings that revealed the

strong relationship between carbonation depth and water sorptivity [38], which depends on the w/c ratio as well as the cement and aggregate contents of concrete mixes.

3.3. Compressive strength

The compressive strength of all RMC and PC samples cured for up to 28 days is shown in Fig. 4. PC samples cured in air and water achieved 28-day strengths of up to 55 and 68 MPa, respectively. The higher strengths demonstrated by PC samples cured under water was as expected since the lack of water in air curing may have led to a limited hydration and potential shrinkage accompanied with surface cracking [39]. Subjecting RMC sample M40-0.55 to accelerated carbonation led to similar 28-day strengths of up to 62 MPa. This is a clear indication that RMC samples are able to achieve similar strengths to PC samples when the right mix design and curing conditions are provided. In PC samples, the hydration process and the formation of major hydrate phases such as C-S-H leads to strength gain [40], whereas RMC formulations rely on the progress of carbonation and the associated development of a dense carbonate network [9].

The effect of water content on the strength development of RMC samples can be observed via a comparison of samples M40-0.55 and M40-0.65 with the control sample M40-0.6, as shown in Fig. 4(a). Reducing the w/c ratio from 0.6 to 0.55 led to a constant increase in the strength of RMC samples at all curing durations. A similar trend was observed when the w/c ratio was increased from 0.6 to 0.65, leading to a reduction in strength at all durations. Accordingly, 28-day strength values of 62, 45 and 32 MPa were achieved by samples M40-0.55, M40-0.6 and M40-0.65, respectively. This particular trend observed in strength development can be explained by the reduction in the porosity of samples over time due to the continuous progress of carbonation [12]. Another factor influencing the rate and degree of carbonation is the diffusion rate of CO_2 within the samples, which can be determined by the water content and the saturation rate of pores. Mixes with higher water contents (w/c of 0.65) can demonstrate a slower

diffusion of CO_2 due to the saturated pore network, thereby leading to lower strength gain. Decreasing the water content (w/c of 0.55) not only led to samples with a lower initial porosity but may have also increased the diffusion of CO_2 within the samples, thereby leading to higher strength gains.

The effect of cement content on the strength development of RMC samples can be observed via a comparison of samples M35-0.6 and M45-0.6 with the control sample M40-0.6, as shown in Fig. 4(b). An increase in the RMC content from 35% to 45% generally resulted in an increase in the compressive strength of all samples, albeit less significantly than the water content. Strengths as high as 52 MPa were achieved by the M45-0.6 sample after 28 days, which was 16% higher than the corresponding strength of the control sample (45 MPa). Alternatively, a similar reduction in the water content led to a 38% increase in the strength of the control sample by revealing a 28-day strength of 62 MPa, as reported earlier. This is mainly because the main issue in RMC formulations is the optimization of the use of RMC by enabling the complete carbonation of the cement component. Although a higher cement content can intrinsically lead to slightly higher strengths via the generation of a denser structure, the critical issue of fully utilizing the included cement component by facilitating its participation in the carbonation reaction still remains. Therefore, changing the cement content has a smaller influence on the overall mechanical performance of the designed formulations than other parameters within the mix design that can enable the continuous ingress of CO_2 through the available pore network. This was also further confirmed with a two-way analysis of variance (ANOVA) conducted on the 28-day strength data of the different samples. The significance of each parameter (water and cement content) was investigated via the calculation of the F-ratio. The bigger F-ratio revealed by samples with different water contents as opposed to that of samples with different cement contents (i.e. 3 vs. 1.2) highlighted the larger significance the initial water content had on the strength development of RMC-based concrete formulations.

3.4. XRD

The XRD patterns of RMC samples after 14 days of curing are shown in Fig. 5. Amongst some minor peaks of other phases, the main carbonate phase observed was hydromagnesite as well as a minor formation of dypingite. Many of the strong and weaker peaks of hydromagnesite (PDF #025-0513) could be seen in the XRD patterns presented, confirming its presence. Hydromagnesite has some of its highest intensity peaks at 15.3°, 30.8° and 13.7° 2θ, which are similar to those of dypingite and hence are expected to overlap on the XRD spectra. In addition to HMCs, all selected samples exhibited the presence of unhydrated MgO and uncarbonated brucite. Table 3 lists the quantities of major phases within the pastes extracted from cured samples. All samples indicated hydromagnesite contents ranging between 8-14% of the overall mix composition, whereas the rest was composed of residual MgO (38-55%) and brucite (37-52%). The relatively high contents of the unhydrated MgO were an indication of the low utilization rate of RMC in the hydration and subsequent carbonation reactions. These results clearly imply the potentially higher strengths RMC formulations can achieve if their complete carbonation is realized.

The effect of initial water content was reflected in the degree of hydration expressed in terms of the brucite content. An increase in the water content led to a higher amount of brucite accompanied with a lower residual MgO content, as expected. Alternatively, the hydromagnesite content did not reveal a clear trend with respect to the initial water content. The control sample, M40-0.6, indicated a higher hydromagnesite content than M40-0.55 (11% vs. 8%) although the former had achieved a lower strength (45 vs. 62 MPa). This highlights that strength development is not only dependent on the amount of carbonate phases, but also on the morphology of these carbonates [41]. Considering its lower hydromagnesite content, another factor that may have played a role in the strength development of M40-0.55 was its dense structure achieved via the use of a lower water content than the other mixes. This was also evident from the density and porosity results presented earlier. This outcome was in line with the water sorptivity

results, showing that M40-0.55 revealed a slightly higher water sorptivity than M40-0.6 after carbonation, corresponding to a lower amount of carbonate phases albeit its higher strengths.

Water plays a key role in the continuation of the hydration process, which leads to the formation of brucite that reacts with CO_2 to form carbonate phases. As sample M40-0.55 had a lower water content than other samples, it demonstrated a lower hydration degree (i.e. highest residual MgO content of 55%) due to its limited hydration. This was also reflected as a lower hydromagnesite content as the carbonation reaction is dependent on the extent of the preceding hydration process and the formation of brucite. An opposite effect was seen in samples with higher water contents, which experienced a higher conversion rate of MgO into brucite. However, it must be noted that excessive water present within the pore structure can also prohibit the diffusion of CO_2, leading to a reduction in the extent of carbonation. This can explain the lower hydromagnesite content of sample M40-0.65 than M40-0.6 (10 vs. 11%) in spite of its initially higher brucite content (52 vs. 42%).

In line with the strength results, the phase quantification of samples M35-0.6 and M45-0.6 with different cement contents did not indicate major differences and revealed similar brucite and HMC contents of 43-45% and 13-14%, respectively. These were consistent with the previous findings, showing that changing the cement content did not have a major influence on the contents of the final phases and sample performance as a majority of the initially used RMC remained unutilized.

3.5. TGA/DSC

The TGA and DSC curves of RMC samples after 14 days of accelerated curing are presented in Fig. 6. Three major decomposition steps in accordance with the previous literature [42-48] were identified as:

(i) 50 to 320 °C: Dehydration of water bonded to HMCs ($4MgCO_3 \cdot Mg(OH)_2 \cdot 4H_2O \rightarrow 4MgCO_3 \cdot Mg(OH)_2 + 4H_2O$ [42, 44, 46-48].

(ii) 320 to 480 °C: Dehydroxylation of HMCs ($4MgCO_3 \cdot Mg(OH)_2 \rightarrow 4MgCO_3 + MgO + H_2O$) and decomposition of uncarbonated brucite ($Mg(OH)_2 \rightarrow MgO + H_2O$) [43, 44, 46, 48].

(iii) 480 to 900 °C: Decarbonation of HMCs ($MgCO_3 \rightarrow MgO + CO_2$) [44, 46].

Table 4 lists the weight losses associated with each reaction taking place at the temperature ranges listed above, along with the corresponding H_2O and CO_2 contents of all RMC samples. The loss of H_2O associated with brucite decomposition was differentiated from the dehydroxylation process of HMCs that took within the same temperature range via the data presented earlier in Table 3. The total weight loss increased with the water content, which was associated with a higher brucite content. In line with the XRD quantification results, sample M40-0.6 revealed a higher CO_2 loss corresponding to a higher HMC content than corresponding samples with different water contents (M40-0.55 and M40-0.65). This was consistent with earlier explanations highlighting the importance of the morphology of the carbonate phases, rather than their content, in strength development. Alternatively, variations in the cement content did not influence the total CO_2 content of different samples, which was almost the same at around 15% for all three samples. The similar total weight losses (39%) revealed by these samples were in line with the strength results, indicating a direct relationship between the extent of hydration and carbonation reactions and mechanical performance.

3.6. Microstructure

Fig. 7 shows the microstructural images of the two best performing RMC-based samples M40-0.55 and M40-0.6 after 14 days of curing. The main carbonate phase observed in both samples was hydromagnesite, which is defined by its rosette-like structure. As also reported earlier by the XRD and TGA results, hydromagnesite was accompanied with brucite and periclase crystals. When compared to M40-0.6, M40-0.55 revealed a denser and more closely packed formation of hydromagnesite, which could explain its higher strength results. These microstructures were supported with an elemental composition analysis of the same samples shown in Fig. 8. The details of the composition of each sample are listed in Table 5. Similar to the XRD and TGA quantification results, sample M40-0.6 revealed a higher carbon content than the corresponding sample M40-0.55, in spite of its lower strength.

This can be explained via a consideration of all factors that influence the microstructural evolution and thereby the performance of RMC formulations. One of the main factors that contribute to the network structure is the binding strength and morphology of carbonates [14, 15]. The inter-connected and well-developed HMC crystals give rise to the formation of a strong network, leading to improved strength. Another important factor is the reduction in the initial porosity and associated microstructure densification caused by the expansive formation of carbonate phases via the reaction between brucite and CO_2. This was confirmed by the rapid reduction in porosity, increase in density and strength development of RMC samples during the first seven days of carbonation.

When all the aforementioned factors are considered, it is evident from the presented results that the initial water content within the samples had a significant influence on the overall porosity. A reduction in the water content enabled lower porosities. This had a direct influence on the final strength of samples and was evidently more crucial than the total carbonation degrees achieved by each sample.

3.7. Thermal conductivity

Mix design, including the cement, aggregate and water content, as well as the curing conditions have a direct influence on the thermal conductivity of concrete [5, 49]. Table 6 lists the thermal conductivity values of all samples after 7 days of curing. The thermal conductivities of RMC samples were higher than corresponding PC samples due to the different cementitious components in each system. Amongst RMC samples, the thermal conductivity noticeably increased with increasing water content. This was associated with the larger porosity of samples with higher water contents, leading to higher conductivities [50, 51]. Samples M35-0.6 and M40-0.6 revealed similar conductivity values, whereas a further increase in the cement content in sample M45-0.6 led to a decrease in thermal conductivity. This could be because of the lower aggregate content of sample M45-0.6 when compared to M35-0.6 and M40-0.6. The cement binder generally possesses a lower thermal conductivity than aggregates. A reduction in the aggregate content may have led to a decrease in the thermal conductivity of M45-0.6 [52].

4. Conclusions

This study presented the influence of mix design on the hydration and carbonation potential of RMC-based concrete samples in comparison to PC-based samples. The two main parameters investigated in this study (i.e. water and cement contents) not only influenced the initial density, porosity and thereby the final performance of the designed formulations, but also other parameters such as their thermal conductivity. The initial water content was determined as the main parameter controlling the final properties of RMC samples, which demonstrated a substantial increase in their density and an associated decrease in porosity over 28 days of curing due to the expansive formation of carbonate phases. A majority of this change took place during the first 7 days,

showing that the carbonation process relatively slowed down afterwards. Alternatively, PC samples revealed negligible changes in their density and porosities due to the different strength gain mechanisms the two binder systems relied upon.

The compressive strength of RMC samples increased with a reduction in the w/c ratio. This was associated with lower porosities of the drier samples, along with the faster diffusion of CO_2 within dry mediums. Sample M40-0.55 (i.e. containing 40% cement and 60% coarse aggregates at a w/c ratio of 0.55) revealed the highest increase in density and the lowest porosity after carbonation and achieved the highest strength out of all the RMC samples, reaching 62 MPa at 28 days. When compared to samples with lower strength results, the lower amount of phase formations obtained in this sample highlighted the importance of the initial mix design that directly influenced the porosity and controlled the overall strength development. Strengths of RMC samples were comparable with those of PC samples cured in air (55 MPa) and water (68 MPa), showing that RMC-based concrete can compete with PC-based concrete in terms of mechanical performance, even without an extensive optimization of its strength gain process.

Another factor that contributed to the mechanical performance of RMC samples was the morphology of the formed carbonates, rather than their quantity. The densification of the sample microstructures, enabled via the formation of hydrate and carbonate phases that filled in the initially available pore space, was an indication of the extent of the carbonation reaction. The water content as well as the paste volume had a direct influence on these properties by determining the overall pore volume, showing that the carbonation degree can be further increased with the optimization of these parameters. The mechanical performance and associated microstructural development of RMC samples can be further improved with an extensive optimization study focusing on other mix design parameters along with the curing conditions.

Acknowledgement

The authors would like to acknowledge the financial support from the Singapore MOE Academic Research Fund Tier 1 (RG 113/14) for the completion of this research project.

References

[1] X.F. Zhang, S.Y. Zhang, Z.Y. Hu, G. Yu, C.H. Pei, R.N. Sa, Identification of connection units with high GHG emissions for low-carbon product structure design, Journal of Cleaner Production 27 (2012) 118-125.

[2] E. Benhelal, G. Zahedi, E. Shamsaei, A. Bahadori, Global strategies and potentials to curb CO2 emissions in cement industry, Journal of Cleaner Production 51 (2013) 142-161.

[3] D.K. Panesar, L. Mo, Properties of binary and ternary reactive MgO mortar blends subjected to CO2 curing, Cement and Concrete Composites 38 (2013) 40-49.

[4] P. Van den Heede, N. De Belie, Environmental impact and life cycle assessment (LCA) of traditional and 'green'concretes: literature review and theoretical calculations, Cement and Concrete Composites 34(4) (2012) 431-442.

[5] A.M. Neville, Properties of Concrete, 4th, London: Pitman Publishing 687 (1995) 331.

[6] A.J.W. Harrison, Reactive magnesium oxide cements, Google Patents, 2008.

[7] A.J.W. Harrison, B.S.B.E. FCPA, New cements based on the addition of reactive magnesia to Portland cement with or without added pozzolan, Proc., CIA Conference: Concrete in the Third Millenium, CIA: Brisbane, Australia, 2003.

[8] L. Vandeperre, M. Liska, A. Al-Tabbaa, Hydration and mechanical properties of magnesia, pulverized fuel ash, and portland cement blends, Journal of Materials in Civil Engineering 20(5) (2008) 375-383.

[9] C. Unluer, A. Al-Tabbaa, Impact of hydrated magnesium carbonate additives on the carbonation of reactive MgO cements, Cement and Concrete Research 54 (2013) 87-97.

[10] Y. Yi, M. Liska, A. Al-Tabbaa, Properties and microstructure of GGBS–magnesia pastes, Advances in Cement Research 26(2) (2014) 114-122.

[11] M.A. Shand, The chemistry and technology of magnesia, John Wiley & Sons, Hoboken NJ, USA, 2006.

[12] C. Unluer, A. Al-Tabbaa, Enhancing the carbonation of MgO cement porous blocks through improved curing conditions, Cement and Concrete Research 59 (2014) 55-65.

[13] C. Unluer, A. Al-Tabbaa, Characterization of light and heavy hydrated magnesium carbonates using thermal analysis, Journal of Thermal Analysis and Calorimetry 115(1) (2014) 595-607.
[14] L. Mo, D.K. Panesar, Effects of accelerated carbonation on the microstructure of Portland cement pastes containing reactive MgO, Cement and Concrete Research 42(6) (2012) 769-777.
[15] P. De Silva, L. Bucea, D. Moorehead, V. Sirivivatnanon, Carbonate binders: reaction kinetics, strength and microstructure, Cement and Concrete Composites 28(7) (2006) 613-620.
[16] L. Vandeperre, A. Al-Tabbaa, Accelerated carbonation of reactive MgO cements, Advances in Cement Research 19(2) (2007) 67-79.
[17] M. Liska, A. Al-Tabbaa, Performance of magnesia cements in pressed masonry units with natural aggregates: Production parameters optimisation, Construction and Building Materials 22(8) (2008) 1789-1797.
[18] M. Liska, A. Al-Tabbaa, Ultra-green construction: reactive magnesia masonry products, Proceedings of the ICE-Waste and Resource Management 162(4) (2009) 185-196.
[19] C. Unluer, A. Al-Tabbaa, The role of brucite, ground granulated blast furnace slag, and magnesium silicates in the carbonation and performance of MgO cements, Construction and Building Materials 94 (2015) 629-643.
[20] L. Pu, C. Unluer, Investigation of carbonation depth and its influence on the performance and microstructure of MgO cement and PC mixes, Construction and Building Materials 120 (2016) 349-363.
[21] H. Wong, A. Pappas, R. Zimmerman, N. Buenfeld, Effect of entrained air voids on the microstructure and mass transport properties of concrete, Cement and Concrete Research 41(10) (2011) 1067-1077.
[22] Y.F. Houst, F.H. Wittmann, Influence of porosity and water content on the diffusivity of CO2 and O2 through hydrated cement paste, Cement and Concrete Research 24(6) (1994) 1165-1176.
[23] B. Singh, Specific surface of aggregates related to compressive and flexural strength of concrete, ACI Journal Proceedings, 1958, pp. 897-907.

[24] H. Erntroy, B. Shacklock, Design of high-strength concrete mixes, Cement & Concrete Association, 1954.
[25] N. Buenfeld, E. Okundi, Effect of cement content on transport in concrete, Magazine of Concrete Research 50(4) (1998) 339-351.
[26] A. Stock, D. Hannantt, R. Williams, The effect of aggregate concentration upon the strength and modulus of elasticity of concrete, Magazine of Concrete Research 31(109) (1979) 225-234.
[27] BS, EN, 196-3, Methods of testing cement. Determination of setting times and soundness, Brussels: BSI, European Committee for Standardization (CEN) (2016).
[28] ASTM, C1585-04, Standard test method for measurement of rate of absorption of water by hydraulic-cement concretes, ASTM International (2013).
[29] ASTM, C109-16A, Standard test method for compressive strength of hydraulic cement mortars, ASTM, Philadelphia, PA, USA (2016).
[30] R.W. Cheary, A. Coelho, A fundamental parameters approach to X-ray line-profile fitting, Journal of Applied Crystallography 25(2) (1992) 109-121.
[31] M.K. Howlader, M. Rashid, D. Mallick, T. Haque, Effects of aggregate types on thermal properties of concrete, ARPN Journal of Engineering and applied sciences 7(7) (2012) 900-906.
[32] A. Almusallam, M. Maslehuddin, M. Abdul-Waris, M. Khan, Effect of mix proportions on plastic shrinkage cracking of concrete in hot environments, Construction and Building Materials 12(6) (1998) 353-358.
[33] İ.B. Topçu, V.B. Elgün, Influence of concrete properties on bleeding and evaporation, Cement and Concrete Research 34(2) (2004) 275-281.
[34] T. Harada, F. Simeon, E.Z. Hamad, T.A. Hatton, Alkali metal nitrate-promoted high-capacity MgO adsorbents for regenerable CO2 capture at moderate temperatures, Chemistry of Materials 27(6) (2015) 1943-1949.
[35] L. Basheer, J. Kropp, D.J. Cleland, Assessment of the durability of concrete from its permeation properties: a review, Construction and Building Materials 15(2) (2001) 93-103.
[36] A. El-Dieb, Self-curing concrete: Water retention, hydration and moisture transport, Construction and Building Materials 21(6) (2007) 1282-1287.

[37] S. Kolias, C. Georgiou, The effect of paste volume and of water content on the strength and water absorption of concrete, Cement and Concrete Composites 27(2) (2005) 211-216.
[38] J. Bai, S. Wild, B. Sabir, Sorptivity and strength of air-cured and water-cured PC–PFA–MK concrete and the influence of binder composition on carbonation depth, Cement and Concrete Research 32(11) (2002) 1813-1821.
[39] S. Mindess, J.F. Young, D. Darwin, Concrete, Prentice Hall, Englewood Cliffs, NJ, USA, 1981.
[40] V. Rostami, Y. Shao, A.J. Boyd, Z. He, Microstructure of cement paste subject to early carbonation curing, Cement and Concrete Research 42(1) (2012) 186-193.
[41] P. De Silva, L. Bucea, V. Sirivivatnanon, Chemical, microstructural and strength development of calcium and magnesium carbonate binders, Cement and Concrete Research 39(5) (2009) 460-465.
[42] V. Vágvölgyi, R.L. Frost, M. Hales, A. Locke, J. Kristóf, E. Horváth, Controlled rate thermal analysis of hydromagnesite, Journal of Thermal Analysis and Calorimetry 92(3) (2008) 893-897.
[43] L.A. Hollingbery, T.R. Hull, The thermal decomposition of huntite and hydromagnesite—A review, Thermochimica Acta 509(1–2) (2010) 1-11.
[44] G. Jauffret, J. Morrison, F. Glasser, On the thermal decomposition of nesquehonite, Journal of Thermal Analysis and Calorimetry 122(2) (2015) 601-609.
[45] R.L. Frost, S. Bahfenne, J. Graham, W.N. Martens, Thermal stability of artinite, dypingite and brugnatellite—Implications for the geosequestration of green house gases, Thermochimica Acta 475(1) (2008) 39-43.
[46] R.L. Frost, S.J. Palmer, Infrared and infrared emission spectroscopy of nesquehonite Mg (OH)(HCO3)· 2H2O–implications for the formula of nesquehonite, Spectrochimica Acta Part A: Molecular and Biomolecular Spectroscopy 78(4) (2011) 1255-1260.
[47] S. Purwajanti, L. Zhou, Y. Ahmad Nor, J. Zhang, H. Zhang, X. Huang, C. Yu, Synthesis of magnesium oxide hierarchical microspheres: a dual-functional material for water remediation, ACS Applied Materials and Interfaces 7(38) (2015) 21278-21286.

[48] P. Ballirano, C. De Vito, V. Ferrini, S. Mignardi, The thermal behaviour and structural stability of nesquehonite, MgCO3· 3H2O, evaluated by in situ laboratory parallel-beam X-ray powder diffraction: new constraints on CO2 sequestration within minerals, Journal of Hazardous Materials 178(1) (2010) 522-528.
[49] P. Morabito, Measurement of the thermal properties of different concretes, High Temperatures. High Pressures 21(1) (1989) 51-59.
[50] J. Wong, F. Glasser, M. Imbabi, Evaluation of thermal conductivity in air permeable concrete for dynamic breathing wall construction, Cement and Concrete Composites 29(9) (2007) 647-655.
[51] F. Collet, S. Prétot, Thermal conductivity of hemp concretes: Variation with formulation, density and water content, Construction and Building Materials 65 (2014) 612-619.
[52] K.-H. Kim, S.-E. Jeon, J.-K. Kim, S. Yang, An experimental study on thermal conductivity of concrete, Cement and Concrete Research 33(3) (2003) 363-371.

List of Tables:

Table 1 Chemical composition and physical properties of RMC and PC

	Chemical composition (%)							Physical properties	
	MgO	SiO_2	CaO	R_2O_3	K_2O	Na_2O	LOI	Specific gravity (g/cm^3)	Specific surface area, (m^2/g)
RMC	>91.5	2.0	1.6	1.0	-	-	4.0	3.0	16.3
PC	0.9	20.9	66.2	10.0	0.5	0.1	1.1	3.1	-

Table 2 Mix compositions prepared under this study

Mix	Mix composition (%)			w/c ratio	Curing condition
	PC	RMC	Coarse aggregates		
PC-air	40	0	60	0.33	Air
PC-water					Water
M40-0.55	0	40	60	0.55	Accelerated CO_2
M40-0.6				0.60	
M40-0.65				0.65	
M35-0.6		35	65	0.60	
M45-0.6		45	55	0.60	

Table 3 Quantification of major phases within samples cured for 14 days

Mix	MgO (%)	Brucite (%)	Hydromagnesite (%)
M40-0.55	54.8	37.4	7.9
M40-0.6	46.9	41.9	11.3
M40-0.65	38.0	52.0	10.0
M35-0.6	43.5	42.6	13.9
M45-0.6	41.8	44.9	13.3

Table 4 Weight loss of samples obtained by TGA after 14 days of curing

Mix	Weight loss (wt.%)					
	50-320 °C	320-480 °C	480-900 °C	H_2O (brucite)	CO_2 (HMCs)	Total
M40-0.55	7.8	23.4	3.1	11.6	14.9	34.3
M40-0.6	10.7	25.3	3.2	13.0	15.4	39.1
M40-0.65	10.5	26.2	3.0	16.1	13.1	39.8
M35-0.6	10.6	25.2	3.3	13.2	15.3	39.1
M45-0.6	10.1	25.7	3.2	13.9	14.9	39.0

Table 5 Elemental composition analysis of selected samples after 14 days of curing

Mix	C (%)	O (%)	Mg (%)	Impurities (%)
M40-0.55	12.3	50.1	34.1	3.5
M40-0.6	14.6	40.3	30.6	14.5

Table 6 Thermal conductivity of samples after 7 days of curing

	M40-0.55	M40-0.6	M40-0.65	M35-0.6	M45-0.6	PC-air	PC-water
Thermal conductivity (w/mk)	1.79	2.01	2.17	1.97	1.87	1.40	1.26

List of Figures:

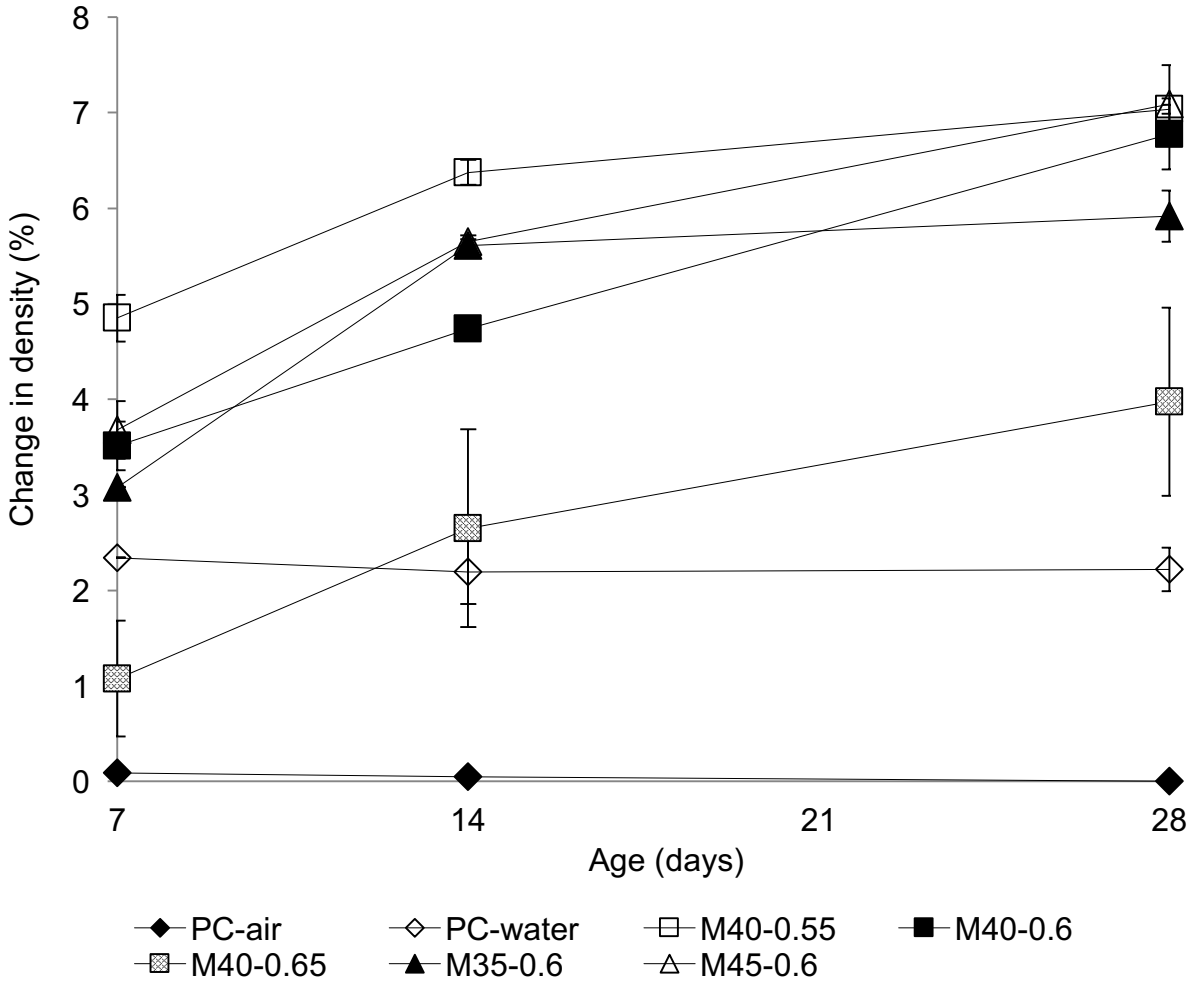

Fig. 1 Change in the density of samples cured for up to 28 days

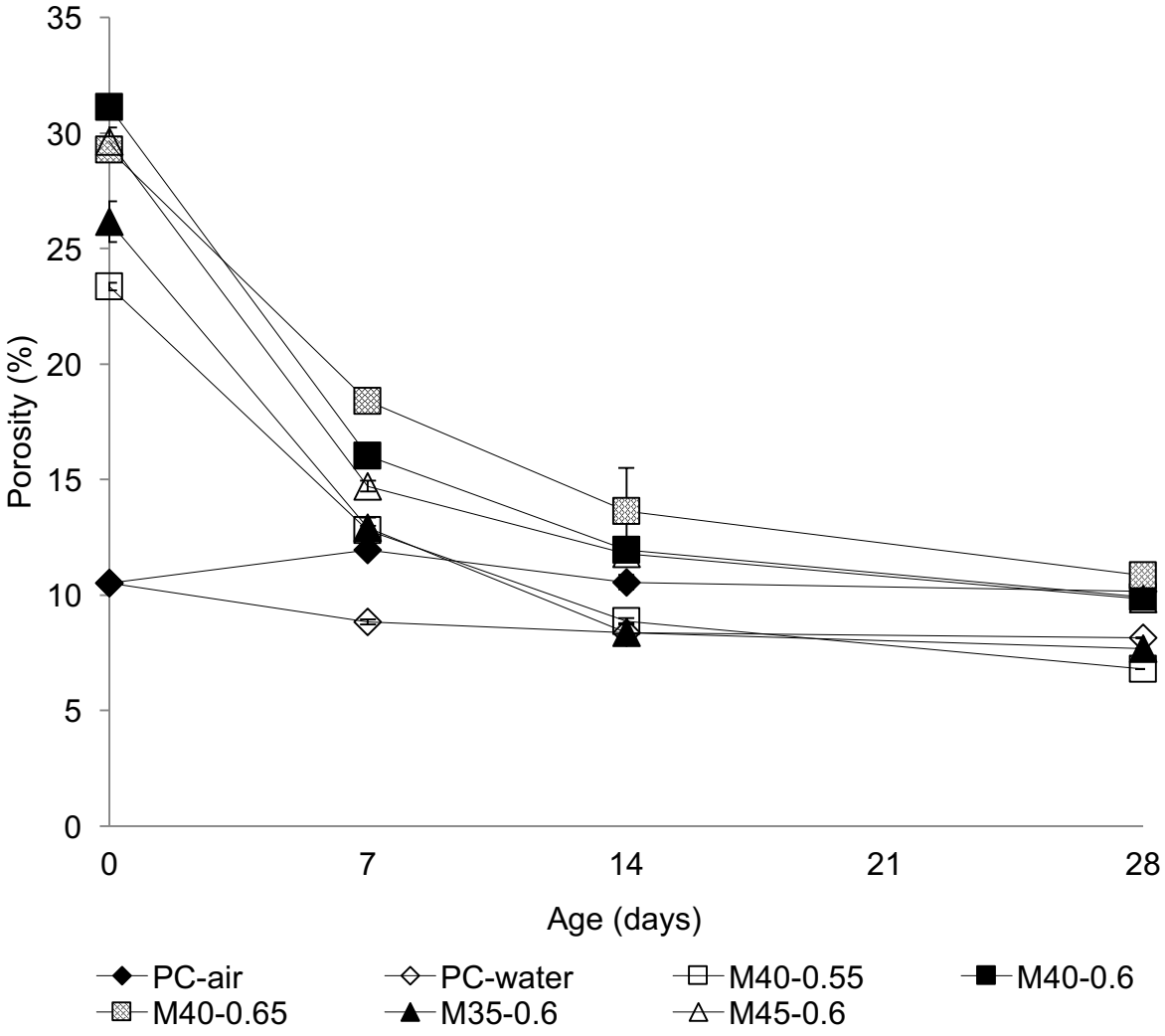

Fig. 2 Porosity of samples cured for up to 28 days

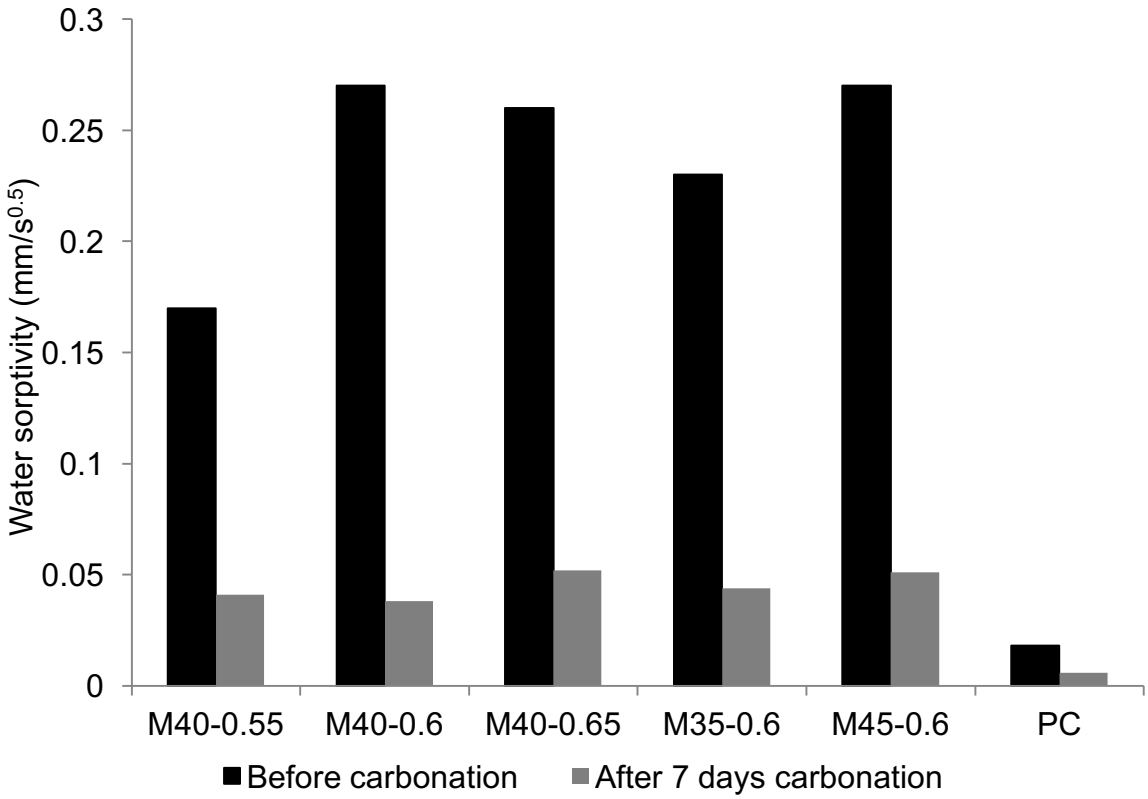

Fig. 3 Water sorptivity of samples before and after 7 days of curing

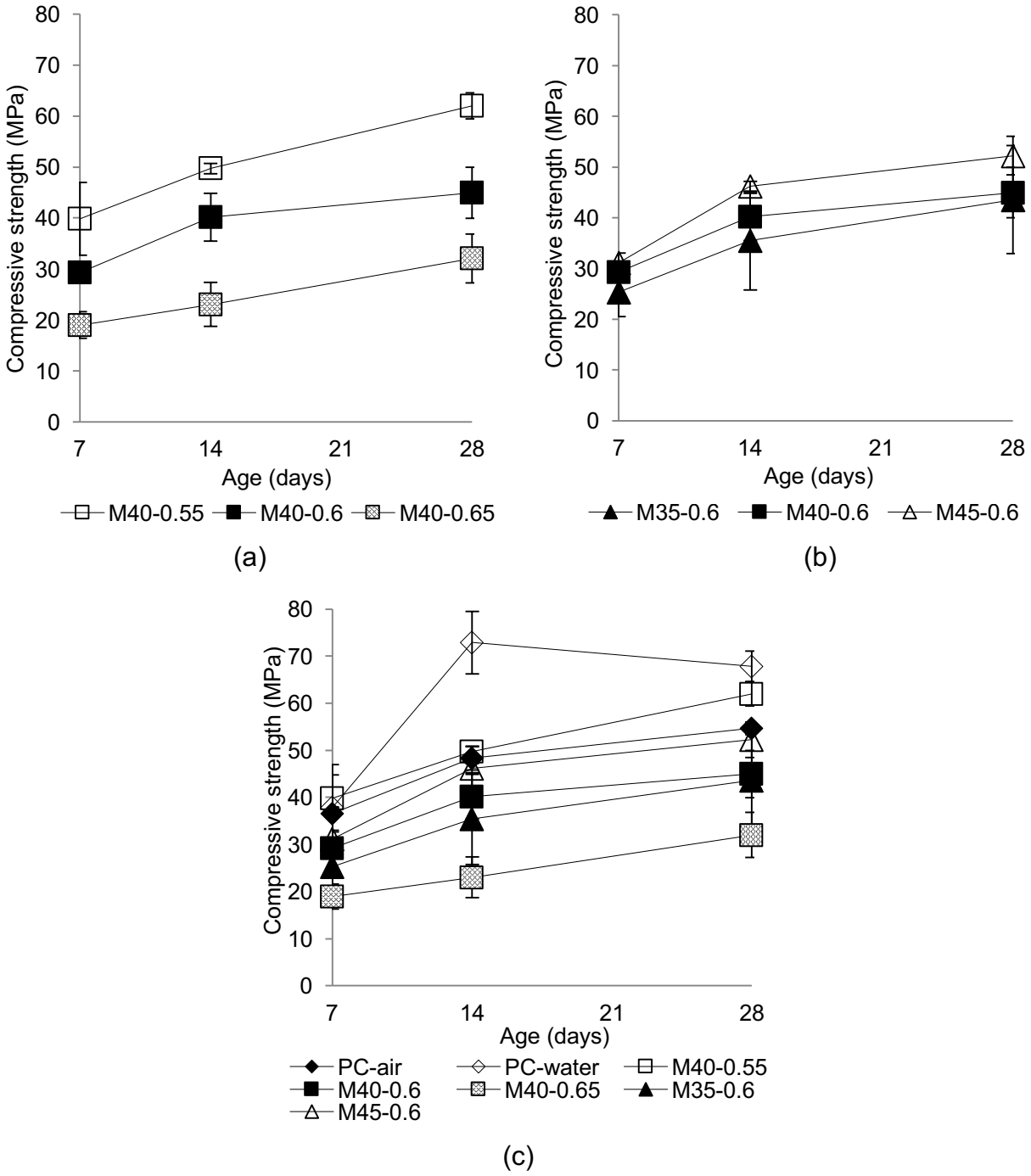

Fig. 4 Compressive strength of samples cured for up to 28 days showing (a) samples with different water contents, (b) samples with different cement contents and (c) all samples

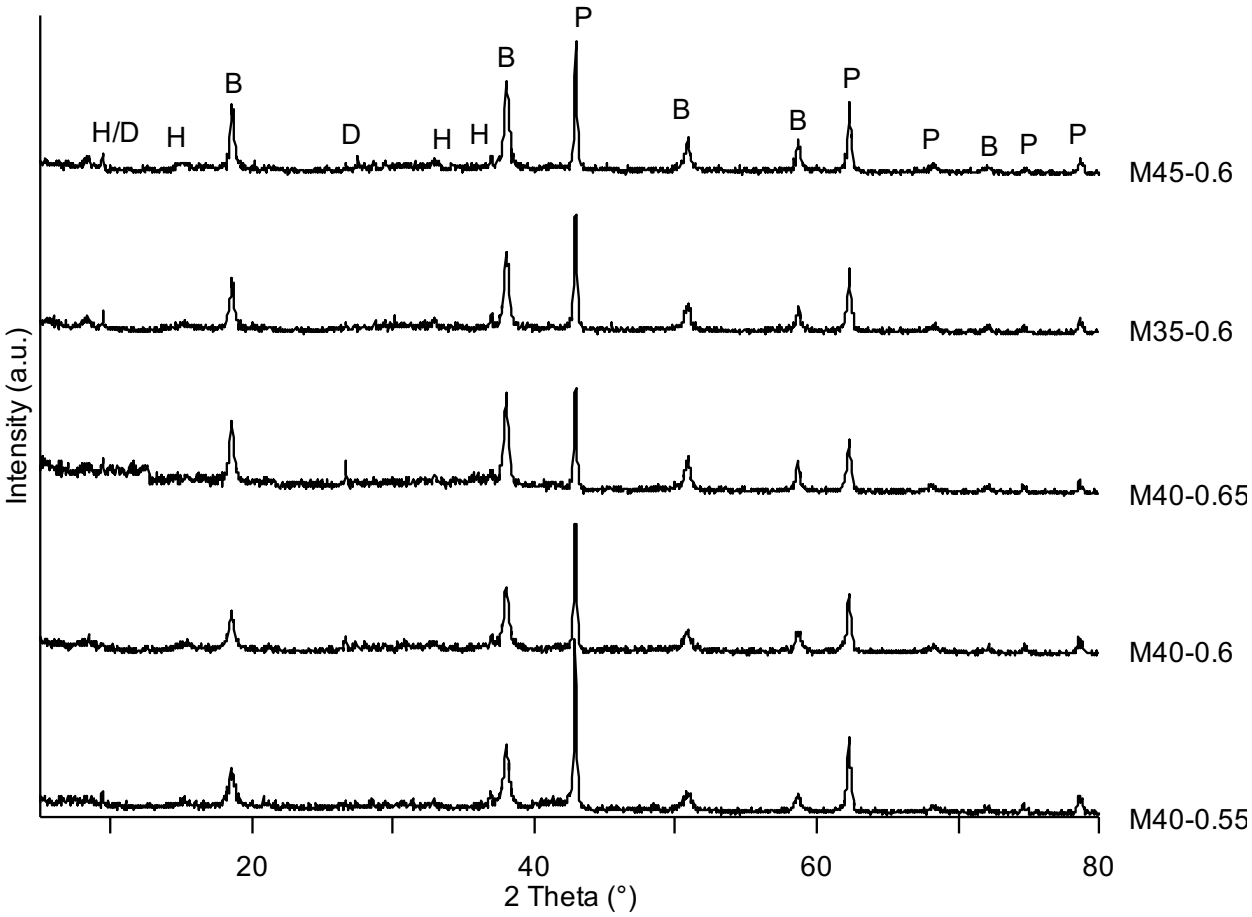

Fig. 5 XRD patterns of RMC samples after 14 days of curing (B: Brucite, H: Hydromagnesite, D: Dypingite, P: Periclase)

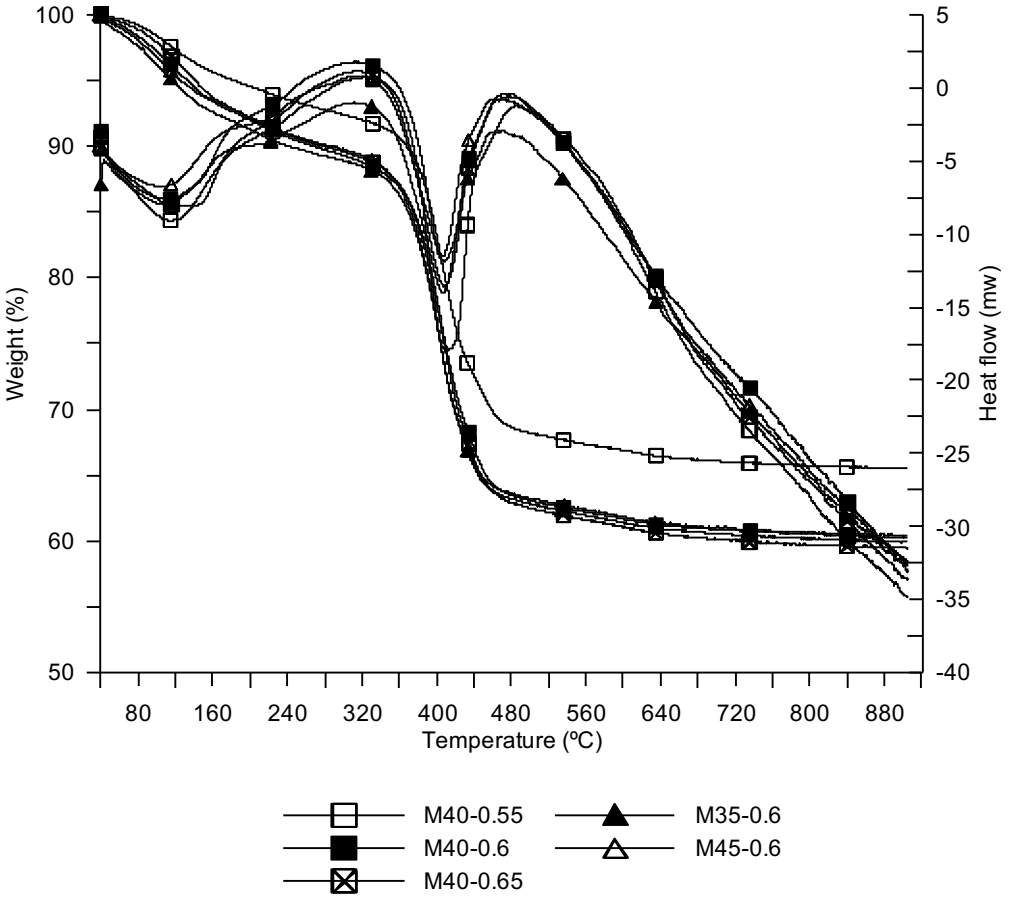

Fig. 6 TGA and DSC curves of RMC samples after 14 days of curing

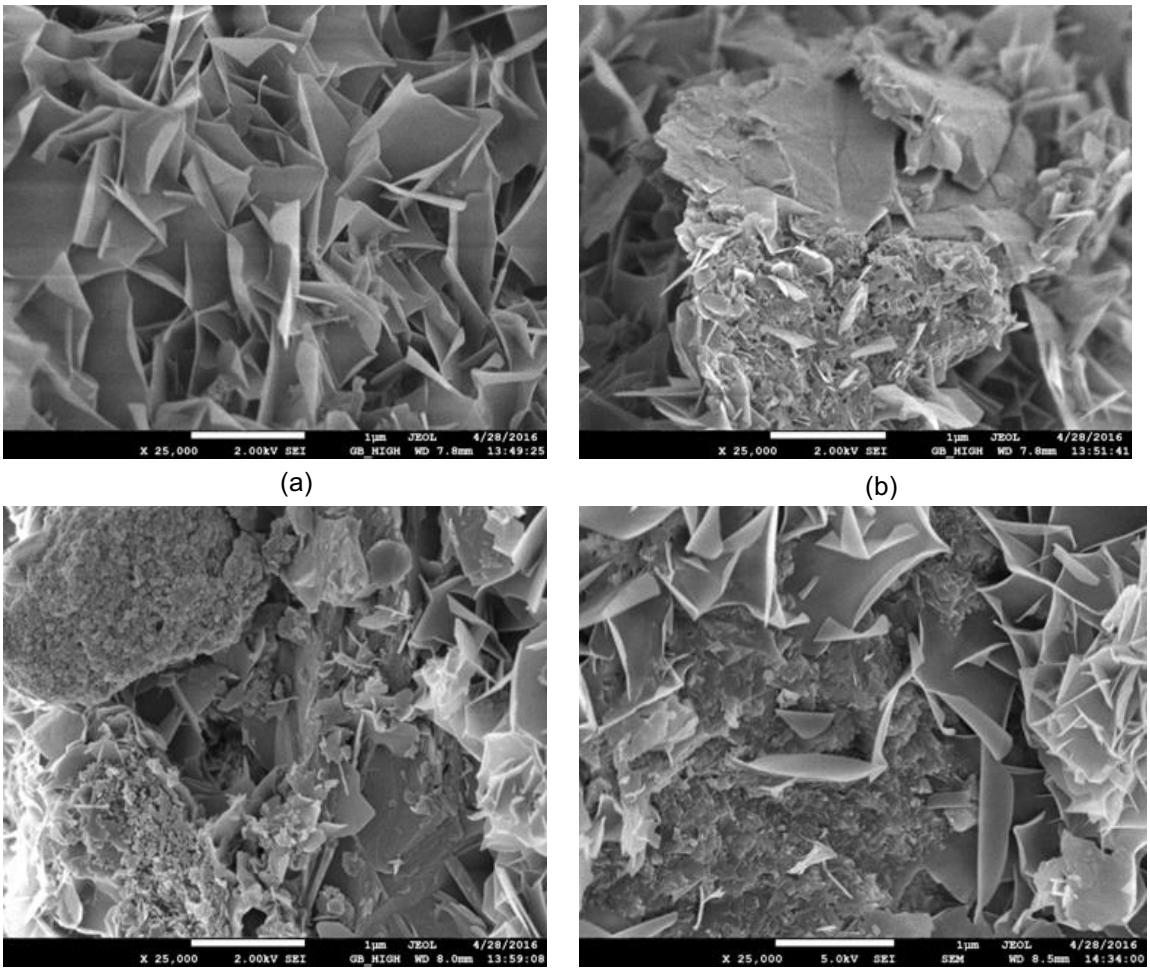

(a) (b)

(c) (d)

Fig. 7 Microstructural images of samples cured for 14 days (a)-(b) M40-0.55 and (c)-(d) M40-0.6

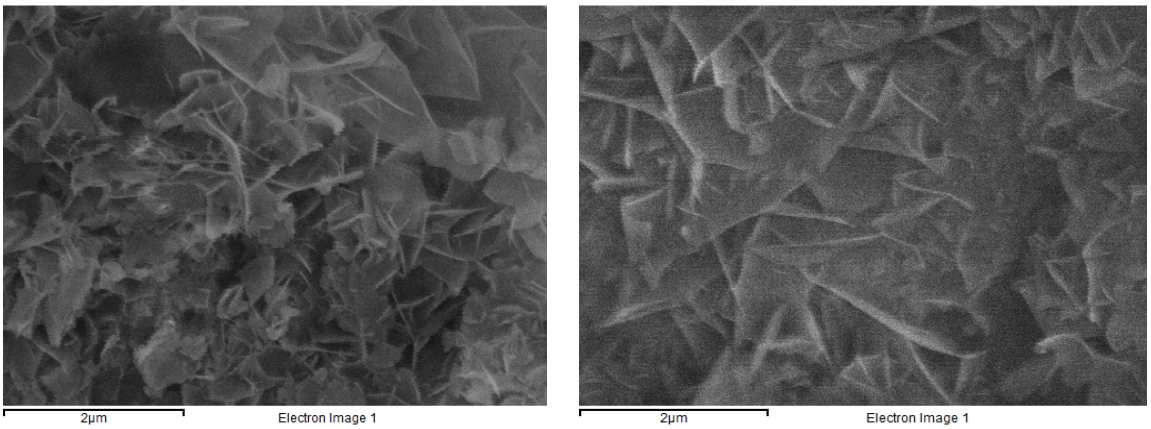

(a) (b)

Fig. 8 Microstructural images taken for the elemental composition analysis of samples cured for 14 days (a) M40-0.55 and (b) M40-0.6